

Journal of Materials Chemistry C

Accepted Manuscript



This article can be cited before page numbers have been issued, to do this please use: E. Zhou, Q. Zhang, B. Xiao, M. Du, G. Li and A. Tang, *J. Mater. Chem. C*, 2018, DOI: 10.1039/C8TC03963A.



This is an Accepted Manuscript, which has been through the Royal Society of Chemistry peer review process and has been accepted for publication.

Accepted Manuscripts are published online shortly after acceptance, before technical editing, formatting and proof reading. Using this free service, authors can make their results available to the community, in citable form, before we publish the edited article. We will replace this Accepted Manuscript with the edited and formatted Advance Article as soon as it is available.

You can find more information about Accepted Manuscripts in the [author guidelines](#).

Please note that technical editing may introduce minor changes to the text and/or graphics, which may alter content. The journal's standard [Terms & Conditions](#) and the ethical guidelines, outlined in our [author and reviewer resource centre](#), still apply. In no event shall the Royal Society of Chemistry be held responsible for any errors or omissions in this Accepted Manuscript or any consequences arising from the use of any information it contains.

A₂-A₁-D-A₁-A₂ type non-fullerene acceptors based on methoxy substituted benzotriazole with three different end-capped groups for P3HT-based organic solar cells

Qianqian Zhang^{1,2#}, Bo Xiao^{2,3#}, Mengzhen Du^{1,2}, Gongqiang Li^{1}, Ailing Tang², Erjun Zhou^{*2}*

¹Key Laboratory of Flexible Electronic (KLOFE) & Institute of Advanced Materials (IAM), Jiangsu National Synergistic Innovation Center for Advanced Materials (SICAM), Nanjing Tech University (NanjingTech), 30 South Puzhu Road, Nanjing 211816, P. R. China.

²CAS Key Laboratory of Nanosystem and Hierarchical Fabrication, CAS Center for Excellence in Nanoscience, National Center for Nanoscience and Technology (NCNST), Beijing 100190, P. R. China.

³University of Chinese Academy of Sciences, Beijing 100049, P. R. China.

*E-mail: zhouej@nanoctr.cn; iamgqli@njtech.edu.cn

#These two authors contributed equally to this work.

Abstract:

In the last three years, A₂-A₁-D-A₁-A₂ skeleton is increasingly popular in the design of non-fullerene acceptors (NFAs), which could particularly match well with the classic p-type polymer of poly(3-hexylthiophene) (**P3HT**). In this manuscript, we successfully synthesized three NFAs with this skeleton and named as **BTA100**, **BTA101** and **BTA103**, where BTA units were substituted by methoxy groups and used as the middle electron-accepting unit (A₁). To finetune the energy levels of final BTA-based NFAs, three different electron-deficient building blocks, thiazolidine-2,4-dione (TD), rhodanine (R) and 2-(1,1-dicyanomethylene)rhodanine (RCN), were used as the end groups (A₂) respectively. The introduction of methoxy groups into BTA can upshift the lowest unoccupied molecular orbital (LUMO) energy level of NFAs and realize a high open-circuit voltage (V_{oc}) organic solar cells. In addition, O atom has a weak

interaction with S atom in the neighbouring thiophene ring, which might be able to facilitate the intramolecular charge transfer. The organic solar cells (OSCs) device based on **P3HT:BTAA103** shows a high PCE of 5.31% with V_{OC} of 0.94 V, J_{SC} of $8.56 \text{ mA} \cdot \text{cm}^{-2}$ and FF of 0.66. In addition, it is worthy noted that the V_{OC} of **P3HT:BTAA100** arrived 1.34V, which is one of the highest values for P3HT based solar cells. These results indicate that RCN is also an effective end group to construct NFAs and methoxy substitution is a simple method to improve the V_{OC} for **P3HT**-based OSC devices.

Keywords: benzotriazole; fullerene-free organic solar cells; high open-circuit voltage; methoxy substitution; non-fullerene acceptor

1. Introduction

Bulk-heterojunction (BHJ) type organic solar cells (OSCs) have achieved rapid development in the last decade, which generally contains a p-type material as electron donor and an n-type material as electron acceptor. In particular, the development of non-fullerene acceptors (NFAs)^{1,2} has led to a rapid increase of power conversion efficiencies (PCEs), which has now exceeded 14%^{3,4}. A great advantage of NFA is that their opto-electronic properties could be easily modulated by the design of the chemical structures. At present, there are mainly two kinds of most successful NFAs. The first one is acceptor-donor-acceptor (A-D-A) type low-band gap fused-ring-electron-acceptor (FREA)⁵⁻⁸, where A is 1,1-dicyanomethylene-3-indanone (IC) and its analogs^{3,9-14}. The other one is based on perylene diimides (PDI)¹⁵⁻¹⁸, with linear or multi-arms structures. The highest PCEs of this two NFAs blending with suitable p-type polymers, reached 14.4%¹⁰ and 10.58%¹⁵ respectively. Although this two kinds of NFAs could pair with many p-type polymers, they do not match with the classic p-type polymer of poly(3-hexylthiophene) (**P3HT**). In the P3HT case, these two kinds of NFAs

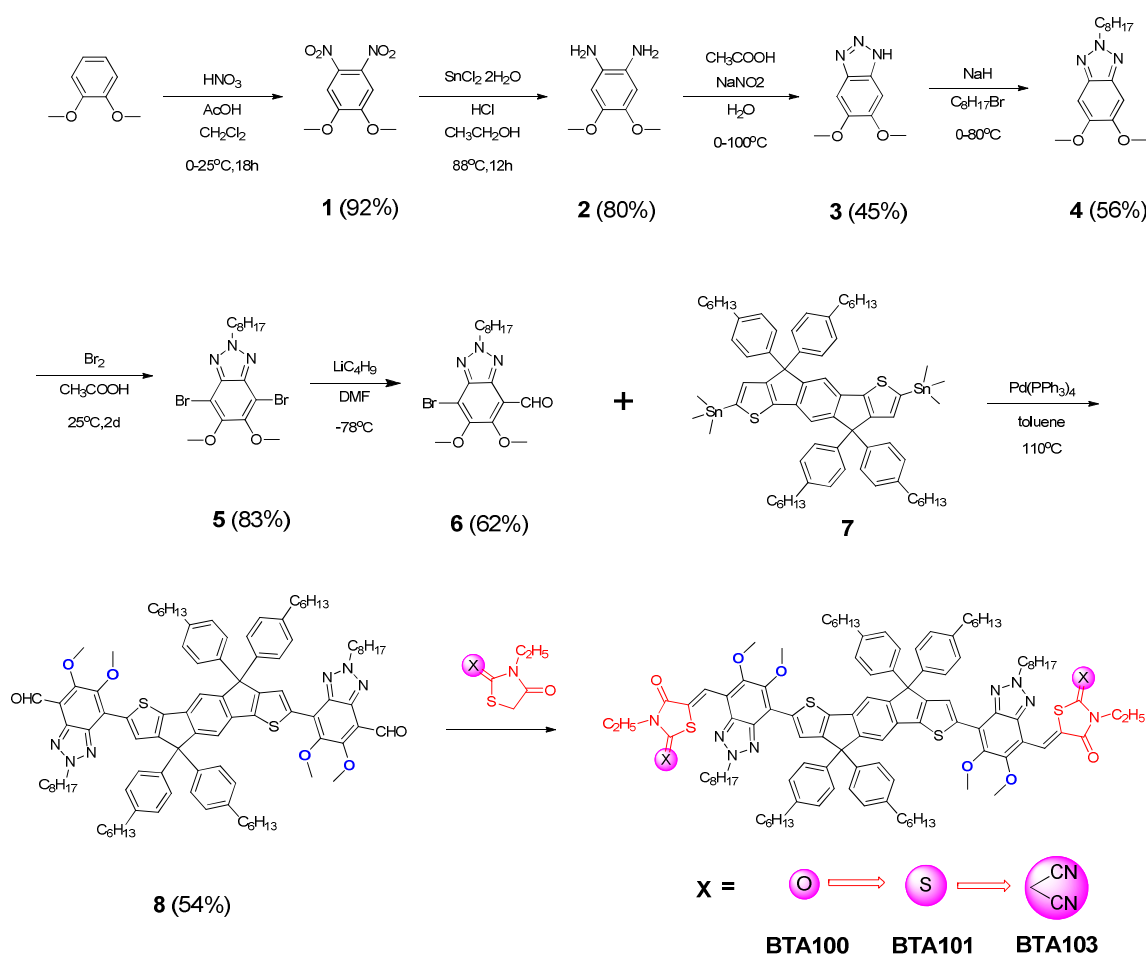
showed inferior photovoltaic performance with the highest PCEs of just 1.25%¹⁹ and 2.61%²⁰, respectively.

In fact, **P3HT** is the most classic photovoltaic donor material, which greatly promotes the development of OSCs. **P3HT** can be synthesized by simple method with large scale, thus is suitable for large-area photovoltaic devices²¹. But the high-lying HOMO of ~5.0 eV and the large band gap of ~1.9 eV result in a low open-circuit voltage (V_{OC}) of ~0.6V and a short-circuit current (J_{SC}) of ~10 mA/cm² for **P3HT:PCBM** system²². Therefore, it is important to design the new acceptor materials that match with **P3HT** perfectly.

The A₂-A₁-D-A₁-A₂ type NFAs²³⁻²⁵ have been proved to match well with **P3HT**. The earliest material is FBR, where fluorene (F), benzothiazole (BT) and rhodanine (R) were used as D, A₁ and A₂ respectively. OSCs based on **P3HT:FBR** realized a PCE of 4.1%.²⁶ After that, the middle unit of D was changed to indacenodithiophene (IDT)²⁷ with different side chains and the final small molecules could realize high PCEs of 5.1-6.4%²⁸⁻³⁰ respectively. In addition, the end-capped segment of A₂ could be further optimized to thiazolidine-2,4-dione (TD) and the final small molecule of **BT2b** could achieve a PCE of 6.08%³¹. However, the V_{OC} of OSCs based on such materials are relatively low. In order to improve the V_{OC} , in our previous works, we introduced the electron-deficient building block of benzotriazole (BTA) to the design of NFAs for the first time. The BTA-based NFAs have high-lying LUMO energy level and the V_{OC} could be largely improved to 1.02 V for BTA1³² and 1.22 V for BTA2²², although the PCEs slightly decreased to 5.24% for BTA1³² and 4.50% for BTA2²². These results indicate BTA-based NFAs are good candidates for **P3HT**-based OSCs.

In order to expand the BTA-based NFAs, in this paper, we introduce methoxy groups to the BTA segment and used it as A₁. To finetune the energy levels of final BTA-based NFAs, three different electron-deficient building blocks, thiazolidine-2,4-dione (TD), rhodanine (R) and 2-(1,1-dicyanomethylene)rhodanine (RCN), were used as the end groups of A₂

respectively. On the one hand, the methoxy group can further increase the LUMO energy level of the material and obtain a high V_{OC} . On the other hand, O atom has a weak interaction with S atom in the neighbouring thiophene ring, which might be able to facilitate the intramolecular charge transfer^{33, 34}. The chemical structures and synthesis method are shown in **Scheme 1**. The effects of end-capped segments on the absorption spectra, energy levels, crystallinity and photovoltaic performance are investigated in detail, and we hope the results could provide important information for the further design of novel NFAs to pair with P3HT.



Scheme 1. Synthesis Routes of Small Molecule acceptors **BTA100**, **BTA101** and **BTA103**.

2. Results and discussion

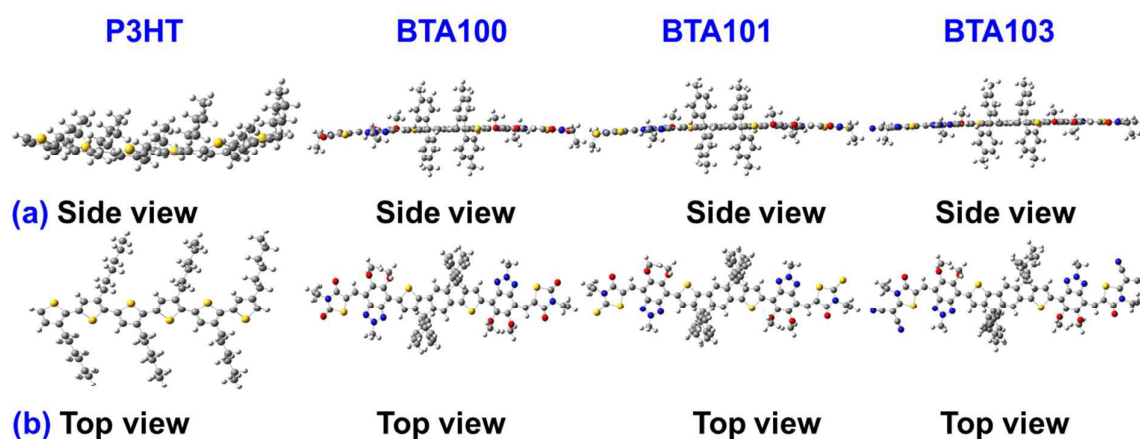
2.1 Synthesis and characterization of BTA100, BTA101 and BTA103

Materials Synthesis. The synthesis routes of three small molecule acceptors **BTA100**, **BTA101** and **BTA103** are depicted in **Scheme 1**. 1,2-dimethoxybenzene was converted to compound **1** initially by nitration reaction. The reduction of compound **1** with stannous chloride in 12 N HCl gave compound **2**³⁵, which was treated immediately with NaNO₂ to afford compound **3**. Alkylation of compound **3** was carried out in N,N-dimethylformamide with sodium hydride and 1-bromooctane in a good yield³⁶. The position of the alkyl group in compound **4** was confirmed by ¹H NMR. The bromination of compound **4** was finished easily by stirring in acetic acid and dichloromethane with liquid bromine for two days at room temperature³⁵. The compound **6** was synthesized by bromine-lithium exchange and then to formyl group³⁷. By using Stille coupling reaction between compound **6** and compound **7** with 2:1 molar ratio, compound **8** with two formyl groups as end groups was obtained, which was then followed by Knoevenagel condensation³⁸ with different end group to give **BTA100**, **BTA101** and **BTA103**. The detailed synthetic procedures are provided in the experimental section of supporting information.

Three small acceptors materials was clearly characterized by ¹H NMR, ¹³C NMR, MALDI-TOF MS spectra, which are shown in **Figure S1**, **S2** and **S3** respectively in the Supporting Information. Furthermore, three small molecules are highly soluble in common chlorinated solvents, such as dichloromethane (DCM), chloroform (CF), chlorobenzene (CB), and o-chlorobenzene (DCB), which makes them feasible to fabricate solution-processed OSC devices.

The structures of the acceptors were calculated by density functional theory (DFT) using Gaussian at the B3LYP/6-31G level of theory, as depicted in **Figure 1**. All the molecules adopt a almost planar geometry, which facilitate the molecular π - π stacking. At the same time, there are four benzene rings with alkyl chains on the side of the plane skeleton, which could effectively prevent the

excessive aggregation of molecules. Through Gaussian calculations, The HOMO/LUMO energy levels are -4.98/-2.81 eV (**BTA100**), -5.05/-2.99 eV (**BTA101**), and -5.21/-3.18 eV (**BTA103**), which indicate the energy levels of BTA-based small molecules could be efficiently downshifted by increasing the electron-withdrawing ability of end-capped groups. The calculated bandgaps of three molecules are 2.17, 2.06 and 2.03 eV, respectively, due to the larger downshift of LUMO than that of the HOMO.



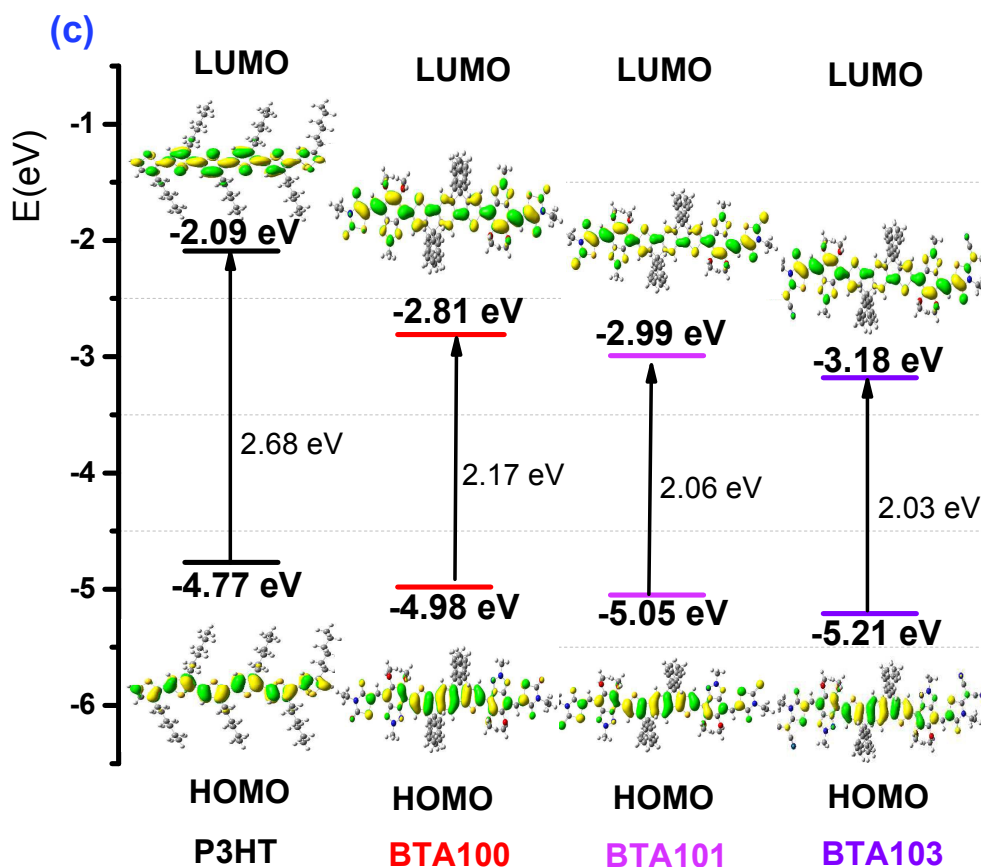


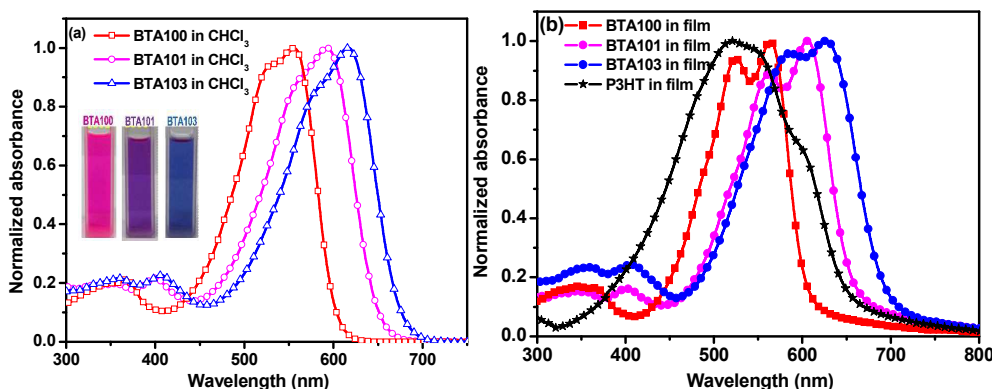
Figure 1. Side view (a) and top view (b) of optimized geometries as well as LUMO and HOMO energy levels (c) of **P3HT**, **BTA100**, **BTA101** and **BTA103**.

Absorption Spectra and Electronic Energy Levels.

The absorption spectra of the **BTA100**, **BTA101** and **BTA103** in CHCl_3 solution and thin film, together with **P3HT** in film for comparison, are shown in **Figure 2a** and **Figure 2b**. **BTA100** in solution showed a broad and strong absorption at the 450-600nm region with a maximum molar extinction coefficient (ϵ) of $1.18 \times 10^5 \text{ L mol}^{-1} \text{ cm}^{-1}$ at 556 nm. Interestingly, **BTA101** has the same coefficient with **BTA100** and maximum absorption at 593 nm in solution, which red-shifted by 37 nm compared with that of **BTA100**. Importantly, the maximum absorption peak of **BTA103** is 617 nm with ϵ of $1.3 \times 10^5 \text{ L mol}^{-1} \text{ cm}^{-1}$, which indicates RCN is an effective end-capped group to improve the absorption spectrum of NFAs. In addition, all the **BTA100**, **BTA101** and **BTA103** films exhibit obvious shoulder peaks and were red-shifted by 8 nm, 13 nm and 10 nm

compared with that in solution, indicating a strong π - π stacking exist in films. Due to the absorption range of **P3HT** located in 400-650 nm, **BTA103** films can form a better complementary absorption than **BTA100** and **BTA101**, which might contribute to improve the short circuit current (J_{SC}) of OSC device. The optical bandgap of **BTA100**, **BTA101** and **BTA103** in thin film are 2.05 eV, 1.88 eV and 1.76 eV, respectively. The corresponding data were summarized in **Table 1**.

The HOMO and LUMO energy levels of **BTA100**, **BTA101** and **BTA103** thin films were measured by electrochemical cyclic voltammetry (CV) and showed in **Figure S4** in the Supporting Information. **BTA100**, **BTA101** and **BTA103** display reversible oxidation and quasi-reversible reduction waves. According to the equations of $LUMO = -e(\phi_{red} + 4.8)$ (eV) and $HOMO = -e(\phi_{ox} + 4.8)$ (eV), where ϕ_{red} and ϕ_{ox} are the onset of reduction and oxidation potentials vs $FeCp_2^{0/+}$, whose absolute energy level is 4.8 eV below vacuum. By calculation, the LUMO/HOMO levels of **BTA100**, **BTA101** and **BTA103** are -3.23/-5.32 eV, -3.55/-5.41 eV and -3.64/-5.37 eV. Since ΔE_{LUMO} (LUMO offset of donor and acceptor) and ΔE_{HOMO} (HOMO offset of donor and acceptor) for **P3HT:BTA101** and **P3HT:BTA103** are beyond 0.3 eV, which can guarantee effective hole and electron transfer. However, ΔE_{LUMO} for **P3HT:BTA100** is just 0.13 eV, which might hinder the hole transfer from **P3HT** to **BTA100**.



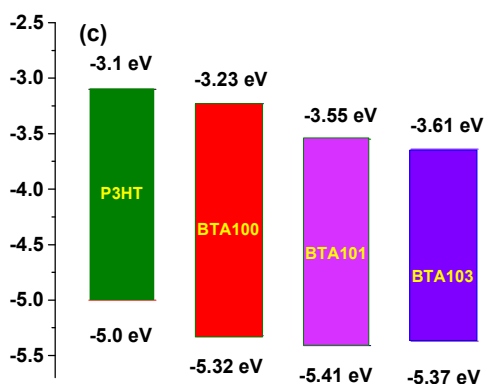


Figure 2. a) The normalized UV-vis absorption spectra of **BTA100**, **BTA101** and **BTA103** in CHCl_3 solution and b) together with **P3HT** in film; c) Energy level diagrams of **P3HT**, **BTA100**, **BTA101** and **BTA103**.

Table 1. The optoelectronic properties of **BTA100**, **BTA101** and **BTA103**

Acceptor	ϵ ($\times 10^5 \text{ L} \cdot \text{mol}^{-1} \cdot \text{cm}^{-1}$)	λ_{max}^a (nm)	λ_{max}^b (nm)	E_g^{opt} (eV)	HOMO/LUMO(eV) ^c
BTA100	1.18	556	564	2.05	-5.32/-3.23
BTA101	1.18	593	606	1.88	-5.41/-3.55
BTA103	1.30	617	627	1.77	-5.37/-3.64

^a solution. ^b thin film. ^c HOMO and LUMO energy levels were estimated from the cyclic voltammetry measurements carried out on the as-cast thin film with $0.1 \text{ mol} \cdot \text{L}^{-1}$ Bu_4NPF_6 electrolyte acetonitrile.

2.2 Photovoltaic properties of P3HT:BTA100, P3HT:BTA100 and P3HT:BTA103 devices

The fullerene-free OSCs were fabricated with a conventional device structure of ITO/PEDOT:PSS ((poly(3,4-ethylenedioxythiophene):poly-(styrene-sulfonate))/active layer/Ca/Al. The active layer consists of **BTA100**, **BTA101** or **BTA103** as the electron acceptor and **P3HT** as the electron donor. The J-V curves of the optimized devices with different solvents, weight ratios and annealing temperatures were shown in **Figure 3a**. **Table 2** lists the detailed device parameters including V_{OC} , J_{SC} , fill factor (FF) and PCE values. All optimal

photovoltaic parameters are provided for the PSCs in **Figure S5**. The active layers of three combinations have the similar thickness of 80-85 nm. Without additives, the OSC device based on **P3HT:BTA100** shows a high V_{OC} of 1.34 V with low PCE of 1.04%, J_{SC} of 1.65 mA/cm² and FF of 0.47. The device based on **P3HT:BTA101** shows a higher V_{OC} of 1.19 V with PCE of 3.55%, J_{SC} of 5.3 mA cm⁻² and FF of 0.56. Importantly, the PCE of **P3HT:BTA103** device reaches up to 5.31% with a V_{OC} of 0.94 V, and these values are significantly higher than that of PC₆₁BM-based control device (V_{OC} = 0.61 V, PCE = 3.67%). The device optimization results display that although the device of **P3HT:BTA100** blend film achieved the highest voltage of 1.34 eV, it did not achieve the best device performance due to the mismatching LUMO energy levels. However, the device of **P3HT:BTA103** blend film obtained the best photovoltaic results due to good complementary absorption, which indicates that the end-capped group is very important for the design of NFAs. In order to further improve the J_{SC} of photovoltaic device, solvent additive of 1-chloronaphthalene (CN) was tested, but the additive played a negative role for all the three material combinations.

In order to investigate the origin of this difference in J_{SC} , external quantum efficiency (EQE) plots of photovoltaic devices based on **P3HT:BTA100**, **P3HT:BTA101** and **P3HT:BTA103** fabricated with different conditions are shown in **Figure 3b**. All the plots show similar shapes in 300–750 nm regions but with different values. The maximum values of EQE are remarkably increased from 13.4% in **P3HT:BTA100** to 36.5% in **P3HT:BTA101** and further to 51.7% in **P3HT:BTA103**, respectively, indicating that the difference in J_{SC} is the result of different electrical or excitonic processes in the devices.

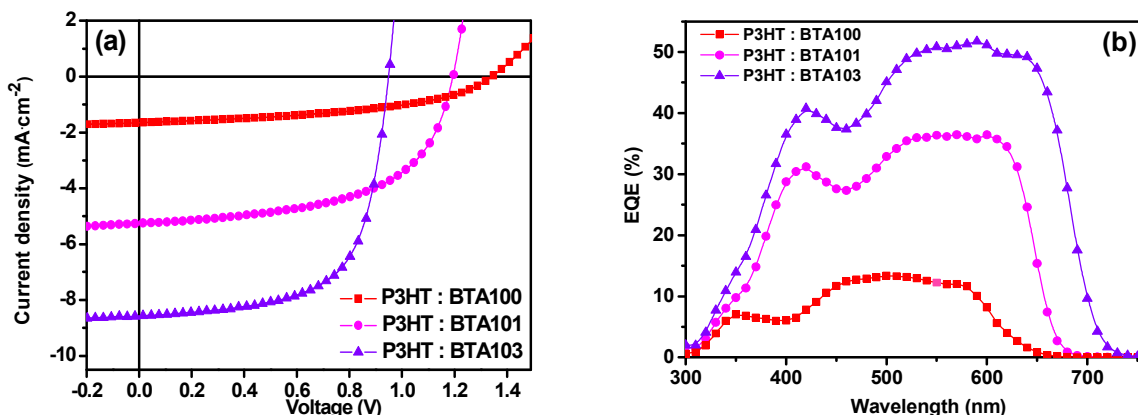


Figure 3. (a) J-V characteristics curves of **P3HT:BTAA100** (1:1, w/w), **P3HT:BTAA101** (1:1, w/w) and **P3HT:BTAA103** (0.5:1, w/w) devices with annealing at 150 °C, 100 °C, 120 °C and 120 °C in turn; and (b) EQE of **P3HT:BTAA100** (1:1, w/w), **P3HT:BTAA101** (1:1, w/w) and **P3HT:BTAA103** (0.5:1, w/w) devices with annealing at 100 °C, 120 °C and 120 °C in turn.

Table 2 Photovoltaic performance of the PSCs based on the **P3HT:BTAA100**, **P3HT:BTAA101** and **P3HT:BTAA103** under the illumination of AM 1.5 G, 100 mW·cm⁻².

Acceptor	Donor	Ratio	Annealing °C	V_{OC} (V)	J_{SC} (mA·cm ⁻²)	FF	PCE _{max} (ave.) ^a
P3HT	BTA100	1:1	100	1.34	1.65	0.47	1.04% (0.90±0.06)
	BTA101	1:1	120	1.19	5.33	0.56	3.55% (3.44±0.14)
	BTA103	1:2	120	0.94	8.56	0.66	5.31% (4.94±0.35)
	PCBM	1:0.8	150	0.61	9.86	0.67	3.67% (3.47±0.11)

^a the average PCE value is calculated form four devices.

The hole mobility and electron mobility of **P3HT:BTAA100** (1:1, w/w), **P3HT:BTAA101** (1:1, w/w) and **P3HT:BTAA103** (0.5:1, w/w) blend film devices were measured using the space charge limited current (SCLC) method. The plots of the J-V curves of the hole-only and electron-only devices are provided in **Figure 4a** and **Figure 4b**, respectively. The hole (μ_h) and electron (μ_e) mobilities of the thermal-annealed **P3HT:BTAA100** film are calculated to be 4.4×10^{-8} cm²·V⁻¹·s⁻¹ and 6.85×10^{-9} cm²·V⁻¹·s⁻¹ respectively, which was lower than that of

P3HT:BTA101 with μ_h of $2.28 \times 10^{-7} \text{ cm}^2 \cdot \text{V}^{-1} \cdot \text{s}^{-1}$ and μ_e of $1.44 \times 10^{-7} \text{ cm}^2 \cdot \text{V}^{-1} \cdot \text{s}^{-1}$. However, the blend film of **P3HT:BTA103** shows higher hole mobility and electron mobility to get $1.46 \times 10^{-6} \text{ cm}^2 \cdot \text{V}^{-1} \cdot \text{s}^{-1}$ and $3.52 \times 10^{-5} \text{ cm}^2 \cdot \text{V}^{-1} \cdot \text{s}^{-1}$. Although the μ_h of **P3HT:BTA103** is slightly low, the high electron transport should contribute to the high PCE because it is helpful to the charge transport and collection in the photovoltaic device.

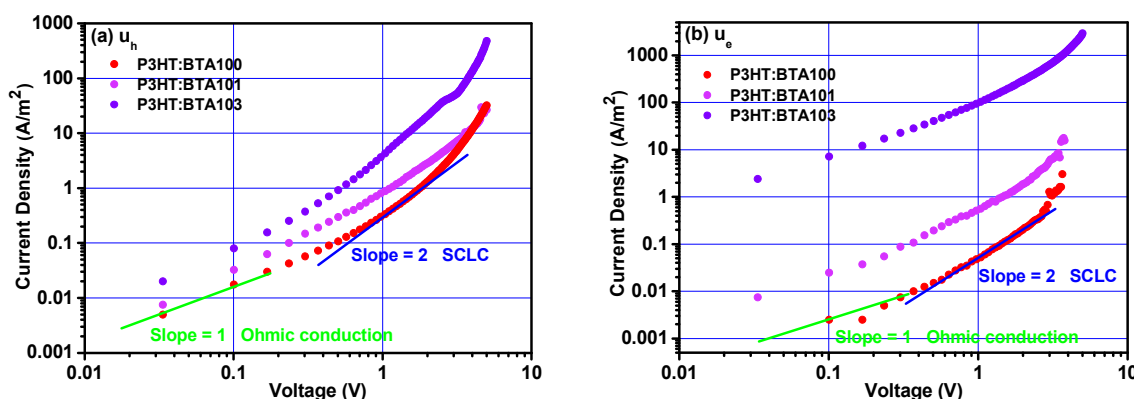


Figure 4. Typical J - V curves based on (a) the hole-only devices of ITO/PEDOT:PSS/ active layer/ Au and (b) the electron-only devices of ITO/ TiOx/ active layer/ Al for electrons.

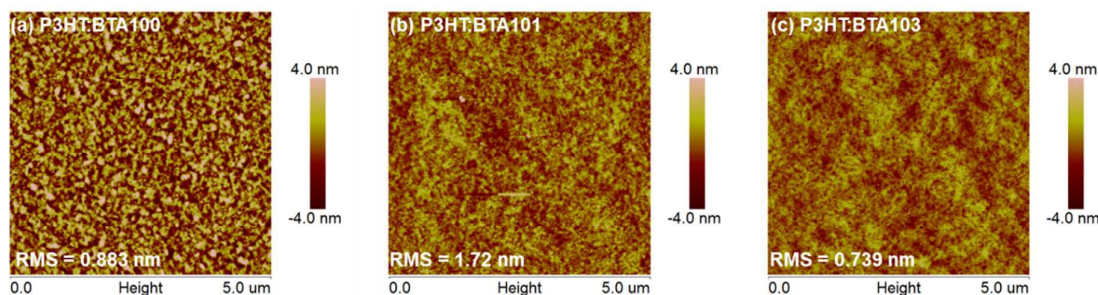
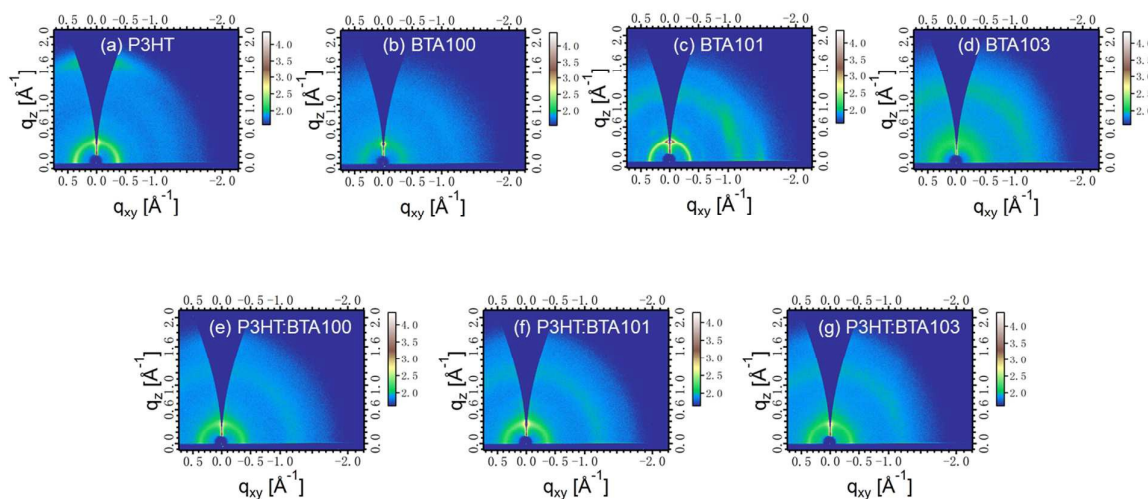


Figure 5. AFM height (top) images ($5 \mu\text{m} \times 5 \mu\text{m}$) of (a) **P3HT:BTA100** (1:1 w/w) blend film annealed at $100 \text{ }^\circ\text{C}$; (b) **P3HT:BTA101** (1:1 w/w) blend film annealed at $120 \text{ }^\circ\text{C}$; (c) **P3HT:BTA103** (0.5:1 w/w) blend film annealed at $120 \text{ }^\circ\text{C}$.

2.3 Morphology of the blend films

The nanoscale morphology of the blend film is one of the important reasons affecting J_{SC} because it can affect the efficiencies of exciton diffusion and exciton dissociation at the donor/acceptor interface as well as free charge transportation

and free charge collection by the electrodes. Atomic force microscopy (AFM) with tapping-mode was utilized to investigate film morphology of the active layers of the OSCs. The height ($5\mu\text{m} \times 5\mu\text{m}$) of annealed blend films are displayed in **Figure 5**. The blend film of **P3HT:BTA100** with annealing at $100\text{ }^\circ\text{C}$ shows a small roughness surface with a root mean square (RMS) roughness of 0.883 nm , however, due to over-stacking and no network interpenetration structure, high short-circuit current and efficiency are not achieved. A similar situation also happened to **P3HT:BTA101** blend film which have a network interpenetration structure but with a relatively rough surface (RMS= 1.72 nm) with annealing at $120\text{ }^\circ\text{C}$. Maybe this is why **P3HT:BTA101** blend film can get higher J_{SC} than **P3HT:BTA100** blend film. Fortunately, the blend film of **P3HT:BTA103** with annealing at $100\text{ }^\circ\text{C}$ shows a small roughness surface with a root mean square (RMS) roughness of 0.739 nm and a network interpenetration structure simultaneously which achieves the greatest J_{SC} and PCE. From the AFM results, it could be concluded that the introduction of **BTA100** into the **P3HT** film resulted in a large phase separation, which is also unfavorable to the J_{SC} of **P3HT:BTA100** device.



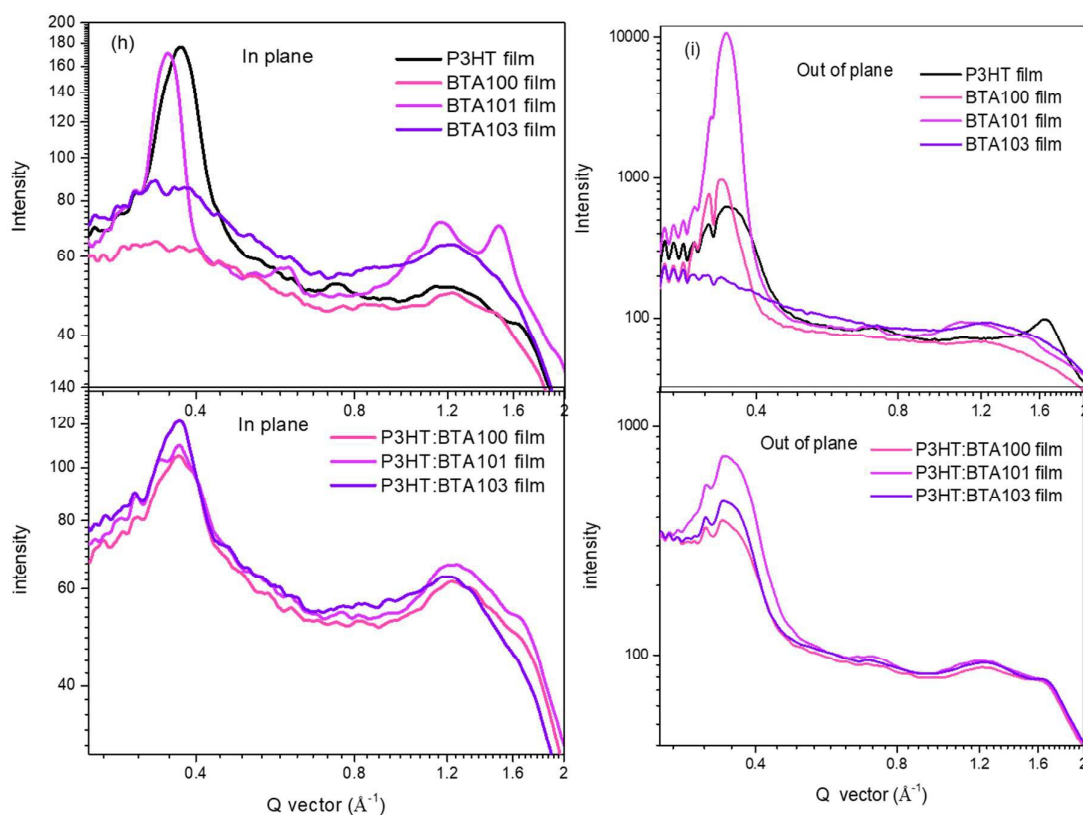


Figure 6. 2D GIWAXS images of (a) (b) (c) (d) the pristine film for **P3HT**, **BTA100**, **BTA101** and **BTA103**; (e) (f) (g) the blend film for **P3HT:BTA100** (1:1 w/w), **P3HT:BTA101** (1:1 w/w) and **P3HT:BTA103** (0.5:1 w/w); (h) (i) In-plane line-cuts and Out-of-plane line-cuts of GIWAXS patterns for **BTA100**, **BTA101** and **BTA103** in different conditions.

The molecular aggregation of the blend films of **P3HT:BTA100** (1:1 w/w), **P3HT:BTA101** (1:1 w/w) and **P3HT:BTA103** (0.5:1 w/w) was further investigated by 2D grazing-incidence X-ray diffraction (GIWAXS). The GIWAXS images and profiles are depicted in **Figure 6**, which represents the intensity profiles versus wave vector q_z and q_{xy} corresponding to the molecular arrangement order in out-of-plane and in-plane directions, respectively. For single component film of **P3HT**, **BTA100**, **BTA101** and **BTA103**, there are strong diffraction peak at 0.37 \AA^{-1} for **P3HT** and 0.35 \AA^{-1} for **BTA101** in plane and out of plane. However, only **P3HT** show clear diffraction peak (010) for π - π stacking at 1.64 \AA^{-1} ($d=3.83 \text{ \AA}$) in out-of-plane. For the blend films, there are strong diffraction peak at 0.37 \AA^{-1} in plane and 0.35 \AA^{-1} out of plane and there is not

clear diffraction peak (010) for π - π stacking, which is not benefit to the charge transport. Further material design to improve the crystallinity of NFAs might be a feasible method to increase the PCEs.

3. Conclusions

In summary, three A_2 - A_1 -D- A_1 - A_2 type small molecule nonfullerene acceptors of **BTA100**, **BTA101** and **BTA103** with three different end groups were designed and synthesized. Due to the electron-withdrawing ability of BTA with the methoxy group unit and end groups, the LUMO orbital of three small molecule acceptors are almost delocalized on all the backbone, which is favorable to electron transport. Because the energy levels and absorption spectrum of **BTA103** matched well with **P3HT**, together with the high electron mobility ($3.52 \times 10^{-5} \text{ cm}^2 \cdot \text{V}^{-1} \cdot \text{s}^{-1}$) and hole mobility ($1.46 \times 10^{-6} \text{ cm}^2 \cdot \text{V}^{-1} \cdot \text{s}^{-1}$), the OSC device based on **P3HT:BTA103** (1:2, w/w) shows a high PCE of 5.31% with V_{OC} of 0.94 V, J_{SC} of $8.56 \text{ mA} \cdot \text{cm}^{-2}$ and FF of 0.66. In addition, although **P3HT:BTA100** (1:1, w/w) shows the highest V_{OC} of 1.34 V, the PCEs is only 1.04% due to the excess small LUMO offset and large phase separation of blend film. Our results indicate that 2-(1,1-dicyanomethylene)rhodanine (RCN) is an effective end group used in the design of NFAs for **P3HT**-based high performance OSC devices.

Acknowledgements

This work is supported by the National Key Research and Development Program of China (2017YFA0206600, 2017YFA0204704), the National Natural Science Foundation of China (Nos. 51473040, 51673048, 21875052, 21602040, 51873044, 51773091, 61604069), the Chinese Academy of Sciences (QYZDB-SSW-SLH033) and Natural Science Foundation of Jiangsu Province (BK20171465)

References

1. C. Yan, S. Barlow, Z. Wang, H. Yan, A. K. Y. Jen, S. R. Marder and X. Zhan, *Nature*

- Reviews Materials*, 2018, **3**, 18003.
2. P. Cheng, G. Li, X. Zhan and Y. Yang, *Nature Photonics*, 2018, **12**, 131-142.
 3. H. Zhang, H. Yao, J. Hou, J. Zhu, J. Zhang, W. Li, R. Yu, B. Gao, S. Zhang and J. Hou, *Adv Mater*, 2018, **30**, 1800613.
 4. Z. Xiao, X. Jia and L. Ding, *Sci. Bullet.*, 2017, **62**, 1562-1564.
 5. J. Wang, J. Zhang, Y. Xiao, T. Xiao, R. Zhu, C. Yan, Y. Fu, G. Lu, X. Lu, S. R. Marder and X. Zhan, *J Am Chem Soc*, 2018, **140**, 9140-9147.
 6. S. Dai, F. Zhao, Q. Zhang, T. K. Lau, T. Li, K. Liu, Q. Ling, C. Wang, X. Lu, W. You and X. Zhan, *J Am Chem Soc*, 2017, **139**, 1336-1343.
 7. Y. Lin, F. Zhao, Q. He, L. Huo, Y. Wu, T. C. Parker, W. Ma, Y. Sun, C. Wang, D. Zhu, A. J. Heeger, S. R. Marder and X. Zhan, *J Am Chem Soc*, 2016, **138**, 4955-4961.
 8. Y. Lin, Q. He, F. Zhao, L. Huo, J. Mai, X. Lu, C. J. Su, T. Li, J. Wang, J. Zhu, Y. Sun, C. Wang and X. Zhan, *J Am Chem Soc*, 2016, **138**, 2973-2976.
 9. N. D. Eastham, J. L. Logsdon, E. F. Manley, T. J. Aldrich, M. J. Leonardi, G. Wang, N. E. Powers-Riggs, R. M. Young, L. X. Chen, M. R. Wasielewski, F. S. Melkonyan, R. P. H. Chang and T. J. Marks, *Adv Mater*, 2018, **30**, 1704263.
 10. S. Zhang, Y. Qin, J. Zhu and J. Hou, *Adv Mater*, 2018, **30**, 1800868.
 11. L. Yang, S. Zhang, C. He, J. Zhang, Y. Yang, J. Zhu, Y. Cui, W. Zhao, H. Zhang, Y. Zhang, Z. Wei and J. Hou, *Chem. Mater*, 2018, **30**, 2129-2134.
 12. W. Zhao, S. Li, H. Yao, S. Zhang, Y. Zhang, B. Yang and J. Hou, *J Am Chem Soc*, 2017, **139**, 7148-7151.
 13. Y. Lin, J. Wang, Z. G. Zhang, H. Bai, Y. Li, D. Zhu and X. Zhan, *Adv. Mater.*, 2015, **27**, 1170-1174.
 14. W. Zhai, A. Tang, B. Xiao, X. Wang, F. Chen and E. Zhou, *Sci. Bullet.*, 2018, **63**, 845-852.
 15. J. Zhang, Y. Li, J. Huang, H. Hu, G. Zhang, T. Ma, P. C. Y. Chow, H. Ade, D. Pan and H. Yan, *J Am Chem Soc*, 2017, **139**, 16092-16095.
 16. M. Li, L. Wang, J. Liu, K. Zhou, X. Yu, R. Xing, Y. Geng and Y. Han, *Phys Chem Chem Phys*, 2014, **16**, 4528-4537.
 17. X. Zhan, Z. Tan, Z. An, X. Zhang, Y. Li and D. Zhu, *J. Am. Chem. Soc.*, 2007, **129**, 7246-7247.
 18. Y. Lin, Y. Wang, J. Wang, J. Hou, Y. Li, D. Zhu and X. Zhan, *Adv Mater*, 2014, **26**, 5137-5142.
 19. Y. Qin, M. A. Uddin, Y. Chen, B. Jang, K. Zhao, Z. Zheng, R. Yu, T. J. Shin, H. Y. Woo and J. Hou, *Adv Mater*, 2016, **28**, 9416-9422.
 20. Y. Lin, J. Wang, S. Dai, Y. Li, D. Zhu and X. Zhan, *Adv. Energy Mater.*, 2014, **4**, 1400420.
 21. R. S. Loewe, S. M. Khersonsky and R. D. McCullough, *Adv. Mater.*, 1999, **11**, 250-253.
 22. B. Xiao, A. Tang, J. Yang, Z. Wei and E. Zhou, *ACS Macro Lett*, 2017, **6**, 410-414.
 23. X. Xu, Z. Bi, W. Ma, Z. Wang, W. C. H. Choy, W. Wu, G. Zhang, Y. Li and Q. Peng, *Adv Mater*, 2017, **29**.
 24. W. Wu, G. Zhang, X. Xu, S. Wang, Y. Li and Q. Peng, *Adv. Funct. Mater*, 2018, **28**, 1707493.
 25. G. Zhang, G. Yang, H. Yan, J. H. Kim, H. Ade, W. Wu, X. Xu, Y. Duan and Q. Peng, *Adv Mater*, 2017, **29**.
 26. S. M. McAfee, J. M. Topple, I. G. Hill and G. C. Welch, *J. Mater. Chem. A*, 2015, **3**, 16393-16408.
 27. Y. Wu, H. Bai, Z. Wang, P. Cheng, S. Zhu, Y. Wang, W. Ma and X. Zhan, *Energy & Environmental Science*, 2015, **8**, 3215-3221.
 28. D. Baran, R. S. Ashraf, D. A. Hanifi, M. Abdelsamie, N. Gasparini, J. A. Rohr, S.

- Holliday, A. Wadsworth, S. Lockett, M. Neophytou, C. J. Emmott, J. Nelson, C. J. Brabec, A. Amassian, A. Salleo, T. Kirchartz, J. R. Durrant and I. McCulloch, *Nat Mater*, 2017, **16**, 363-369.
29. S. Holliday, R. S. Ashraf, C. B. Nielsen, M. Kirkus, J. A. Rohr, C. H. Tan, E. Collado-Fregoso, A. C. Knall, J. R. Durrant, J. Nelson and I. McCulloch, *J Am Chem Soc*, 2015, **137**, 898-904.
30. S. Holliday, R. S. Ashraf, A. Wadsworth, D. Baran, S. A. Yousaf, C. B. Nielsen, C. H. Tan, S. D. Dimitrov, Z. Shang, N. Gasparini, M. Alamoudi, F. Laquai, C. J. Brabec, A. Salleo, J. R. Durrant and I. McCulloch, *Nat Commun*, 2016, **7**, 11585.
31. B. Xiao, A. Tang, L. Cheng, J. Zhang, Z. Wei, Q. Zeng and E. Zhou, *Solar RRL*, 2017, **1**, 1700166.
32. B. Xiao, A. L. Tang, J. Q. Zhang, A. Mahmood, Z. X. Wei and E. J. Zhou, *Adv. Energy Mater.*, 2017, **7**, 1602269.
33. S. H. Park, G. E. Park, S. Choi, Y.-U. Kim, S. Y. Park, C. G. Park, M. J. Cho and D. H. Choi, *J. Mater. Chem. C*, 2018, **6**, 7549-7556
34. S. J. Jeon, S. J. Nam, Y. W. Han, T. H. Lee and D. K. Moon, *Polym. Chem*, 2017, **8**, 2979-2989.
35. M. Helgesen, S. A. Gevorgyan, F. C. Krebs and R. A. Janssen, *Chem. Mater*, 2009, **21**, 4669-4675.
36. J. Min, Z.-G. Zhang, S. Zhang and Y. Li, *Chem. Mater*, 2012, **24**, 3247-3254.
37. A. Tang, B. Xiao, Y. Wang, F. Gao, K. Tajima, H. Bin, Z.-G. Zhang, Y. Li, Z. Wei and E. Zhou, *Adv. Funct. Mater*, 2018, **28**, 1704507.
38. I. Rodriguez, G. Sastre, A. Corma and S. Iborra, *J. Catal*, 1999, **183**, 14-23.

TOC

